

Large-Eddy Simulations of a Sediment-Laden Buoyant Jet Resulting from Dredgers Using Overflow

B. Decrop & M. Sas

International Marine and Dredging Consultants, IMDC, Antwerp, Belgium

T. De Mulder

Ghent University, Dep. of Civil Engineering, Hydraulics Laboratory, Ghent, Belgium

E.A. Toorman

University of Leuven, Dep. of Civil Engineering, Hydraulics Laboratory, Leuven, Belgium

ABSTRACT: Turbidity plumes are an important topic in the environmental aspects of dredging. The main source of turbidity while employing Trailer Suction Hopper Dredgers is the release of excess water through the overflow shaft. In order to minimise environmental impacts of turbidity in early stages of planning as well as during project execution, turbidity prediction tools are necessary. To this end, numerical modelling tools are the most effective in the prediction of the sea currents and sediment dispersion. The near field plume dynamics below and directly behind the sailing hopper dredgers has always been the weakest link in these predictions, since accurate input of the vertical and horizontal distributions of sediment at the source location are paramount to obtain reliable results at the environmentally sensitive areas further away. In this paper, a Computational Fluid Dynamics model is presented as a tool to determine the three-dimensional flows of water, sediment and air bubbles directly after release from the overflow shaft. A full dredger hull geometry and an actuator disk accounting for propeller action add to the representation of the complexity of the flow. It is shown that the model can reproduce two different cases of overflow plumes measured in the field with fair accuracy.

Keywords: Trailer Suction Hopper Dredgers, Turbidity plumes, LES (Large Eddy Simulation), Computational Fluid Dynamics

1 INTRODUCTION

The increase in the number of offshore and port development projects has led to rising dredging activity throughout the world. In order to minimise disruption of natural systems, environmental legislation regulating impacts of dredging works has become more extensive subsequently. Turbidity caused by dredging works with Trailing Suction Hopper Dredgers (TSHD) using an overflow is one of the main environmental concerns being assessed in the phases of planning, design and execution. At sensitive areas near the project, turbidity and sediment depositions rising above the allowed thresholds need to be prevented. Numerical modelling tools are used at the present day to predict circulations in coastal seas as well as advection, settling and diffusion of turbidity plumes (Figure 1)



Figure 1. Example of an overflow plume.

Prediction of the increase in turbidity in the far-field is possible by means of large scale hydraulic and sediment transport models. These models, however, are not designed to solve the complex near field processes in the vicinity of the dredger (since they commonly neglect vertical accelerations, i.e. a hydrostatic pressure distribution is assumed) and require a sediment source term to account for overflow in the form of a distribution of sediment flux over the water depth. Until today, the determination of this distribution has been rather arbitrary. In this study, detailed numerical simulations solving the full three-dimensional Navier-Stokes equations coupled with sediment transport equations allow to predict the sediment plume being released by the overflow pipe underneath the dredging vessel. A laboratory flume was equipped to release scaled dredging plumes. A multiphase large-eddy simulation (LES) model at experimental scale has been validated with laboratory measurements carried out by Decrop *et al.* (2012). The modelled plume trajectory, plume width and turbulent statistics compare well with the experimental data, with trajectory deviations smaller than 0.5 times the overflow pipe diameter D .

The present paper describes the upscaling process of the laboratory-scale LES model to prototype scale, as well as the implementation of a realistic dredging vessel geometry in the model. The surface impinging jet occurring inside the overflow shaft causes air inclusion in the released mixture. Therefore, a gas phase has been implemented in the model to account for the reduction in bulk mixture density and for the momentum exchange between the liquid phase and rising air bubbles. The influence of air bubbles on the behaviour of the plume has been studied by turning on and off the release of air in the numerical model. Also, the pressure jump caused by the two propellers and the consequent propeller jets with related turbulent kinetic energy production are included in the numerical model.

In situ sediment concentration measurements along horizontal and vertical profiles inside a TSHD overflow plume are used to verify the model capability to capture the structure of the plume and the concentration levels at different depths and different distances from the vessel.

2 MODEL EQUATIONS

The multi-phase model consisting of a continuous (sea water) and dispersed phase (fine sediment particles) was set up using the mixture model approach, in which one set of momentum and continuity equations is solved for the mixture only, rather than for each phase. The Navier-Stokes equations are thus written for the mixture and are in conservative form. For LES, the equations are filtered in space with a filter size equal to the grid size. The mixture continuity equation reads:

$$\frac{\partial}{\partial t}(\rho_m) + \nabla \cdot (\rho_m \mathbf{u}_m) = 0 \quad (1)$$

where ρ_m is the mixture density, \mathbf{u}_m is the mass averaged velocity vector of the water-sediment mixture:

$$\mathbf{u}_m = \frac{(1-c)\rho_w \mathbf{u}_w + c\rho_s \mathbf{u}_s}{\rho_m} \quad (2)$$

where c is the sediment volume concentration, ρ_w and ρ_s are the mass density of sea water and sediment, respectively and \mathbf{u}_w and \mathbf{u}_s are the velocity vector of sea water and sediment, respectively. The momentum equation for the mixture reads:

$$\frac{\partial}{\partial t}(\rho_m \mathbf{u}_m) + \nabla \cdot (\rho_m \mathbf{u}_m \mathbf{u}_m) = -\nabla p + \nabla \cdot [\mu(\nabla \mathbf{u}_m + \nabla \mathbf{u}_m^T)] + \rho_m \mathbf{g} + \mathbf{F} + \nabla \cdot \mathbf{D} \quad (3)$$

where p is the pressure, $\mu = \mu_m + \mu_{sgs}$, μ_m is the molecular viscosity of the mixture, μ_{sgs} is the sub-grid scale turbulent viscosity, \mathbf{g} is the gravitational acceleration, \mathbf{F} is a momentum transfer between air bubbles and continuous phase:

$$\mathbf{F} = \frac{18\mu_m C_D Re}{\rho_a d_a^2 24} (\mathbf{u}_a - \mathbf{u}_m) \quad (4)$$

where C_D is a drag coefficient, Re is the air bubble Reynolds number, d_a is the air bubble diameter and \mathbf{u}_a is the air bubble velocity vector.

In LES modeling, the large scales of turbulent eddies are resolved on the model grid. The effect of the remaining smaller scales of turbulent motions, i.e. smaller than the grid size, are included in a sub-grid scale eddy viscosity. To this purpose, the Navier-Stokes equations are filtered with a spatial filter so that only the small scales are filtered away and the larger turbulent motions are allowed to develop in the model results. In most hydrodynamic flow models, to the contrary, the RANS equations are used. These equations are filtered in time, thereby averaging out all turbulent motions. The complex dynamics of a plume in a crossflow such as formed below the keel of a TSDH include time-varying turbulent phenomena such as a von Kármán vortex street and Kelvin-Helmholtz instabilities, e.g. Frick and Roshko (1994), Kelso *et al.* (1996). In order to capture the effect of these flow features on the sediment dispersion, a time domain model is needed which can resolve turbulent motions from the largest scales down to a few decimetres (on prototype scale). The effect of the turbulent scales filtered away is represented by the sub-grid scale turbulent viscosity μ_{sgs} , modelled here using the dynamic Smagorinsky model,

$$\mu_{sgs} = \rho_m \nu_{sgs} = C_s^2 \Delta^2 |S| \quad (5)$$

where C_s is the dynamic Smagorinsky coefficient, derived at each time step at each grid cell from the difference between the grid-filtered (Δ) SGS stress and a test-filtered SGS stress at twice the filter width 2Δ (Germano *et al.*, 1991). S is the rate-of-strain tensor of the mixture .

Since the momentum equation for the mixture (eq. 3) is derived from summing the momentum equations for water and sediment, a drift velocity advection term arises with

$$\mathbf{D} = (1 - c)\rho_w \mathbf{u}_{dr,w} \mathbf{u}_{dr,w} + c\rho_s \mathbf{u}_{dr,s} \mathbf{u}_{dr,s} \quad (6)$$

where velocities with subscript dr are drift velocities of water and sediment phases, defined as the difference between phase velocities \mathbf{u}_w and \mathbf{u}_s on the one hand and the mixture velocity on the other hand.

The slip velocity is defined as $\mathbf{u}_{sw} = \mathbf{u}_s - \mathbf{u}_w$ and is calculated by the expression by Manninen *et al.* (1996) and an extra term for gradient diffusion of the particulate phase.

$$\mathbf{u}_{sw} = \frac{(\rho_s - \rho_m)d_s^2}{18\mu_w} \mathbf{a} - \frac{\nu_{sgs}}{Sc_t} \left(\frac{\nabla c}{c} - \frac{\nabla(1-c)}{1-c} \right) \quad (7)$$

where \mathbf{a} is the acceleration vector, d_s is the diameter of sediment particles and Sc_t is the turbulent Schmidt number for the SGS sediment diffusion, it is derived in a similar way as C_s , from the difference between grid-filtered and test-filtered SGS sediment fluxes (Lilly, 1992).

The SGS diffusion of sediment particles is thus already included in the slip velocity formulation. The dispersed phase transport equation has therefore only the time derivative and advection terms and is written as:

$$\frac{\partial}{\partial t} (\rho_s c) + \nabla \cdot (\rho_s c \mathbf{u}_m) = -\nabla \cdot (\rho_s c \mathbf{u}_{dr,s}) \quad (8)$$

Air bubble volume fractions are tracked using a Lagrangian discrete phase model. In this model, packets of air bubbles are released and the bubbles' trajectories are governed by a force balance including drag force, added mass force and pressure gradient forces in the fluid phase. Turbulent dispersion of air bubbles is handled using a discrete random walk model. Air bubbles experience a bouncing wall boundary condition at the ship hull, and are allowed to escape from the tracking system when reaching the water surface. Coalescence after bubble collision is included in the model, bubble breakup is not.

The source of momentum and turbulent energy ejected by the two propellers of a TSHD is modelled using the concept of an actuator disk, e.g. Hough and Ordway (1964). Over a disk-shaped internal boundary condition, a pressure jump is imposed. The pressure jump Δp_d is a function of the propeller power P , disk surface area A_d and the axial velocity at the disk u_d :

$$\Delta p_d = \frac{P}{A_d u_d} \quad (9)$$

The propeller velocity is also a function of the power, so that the pressure jump can be derived from the propeller power only. Assuming the approach velocity is small compared to u_d , it can be written as:

$$u_d = \sqrt[3]{\frac{P}{2 \rho_m A_d}} \quad (10)$$

The model equations are solved using the Ansys Fluent code, on an unstructured grid in which specific refinements are foreseen for regions of high strain (near ship hull, flow approaching bow, propeller jets) and expected high sediment concentration. The expected high sediment concentration regions are derived from initial steady-state RANS calculations. From these RANS calculations, also a pipe flow velocity profile is extracted to be applied as boundary condition in the LES model. Superimposed on this profile is a velocity variation mimicking vortices passing in time, so that the unsteadiness of the flow is initialised. An example of a slice of the grid along the symmetry plane is given in Figure 2. An overflow shaft section with a length of 5 pipe diameters is included in the computational domain. Inside the shaft mesh, local refinements are foreseen near the wall to resolve the pipe boundary layer.

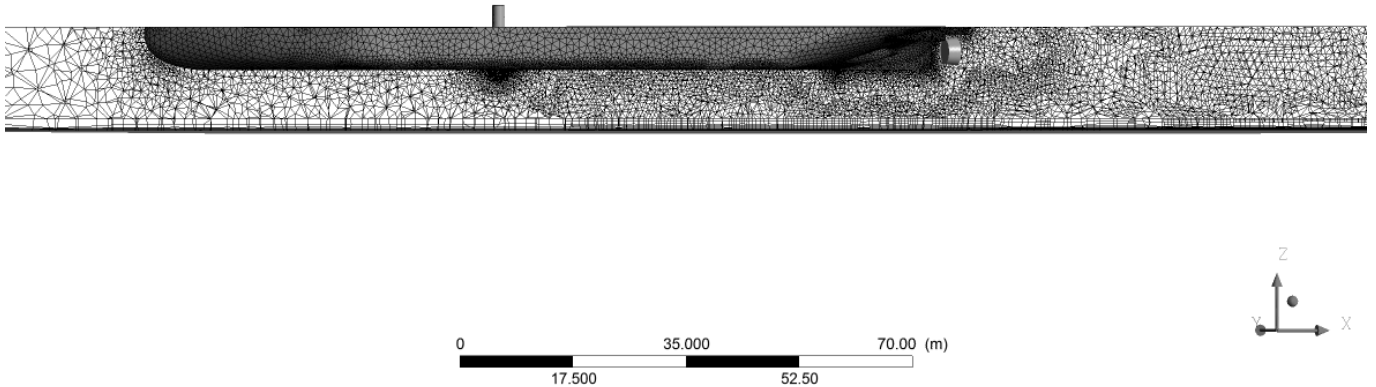


Figure 2. Symmetry plane slice through part of the computational grid near the vessel. The sub-surface part of the vessel hull is visible with the bow at the left and stern at the right, as well as local refinements at the bow, plume exit, at hull curvature regions upstream of the propeller intake and in zones to be occupied by the plume.

The LES model was run with a timestep of 200 milliseconds, to reach a maximum Courant number near the plume exit of about 1.9. At each model run, the simulation was carried out with stationary background flow for the time the flow needs to travel through the complete length of the model (700 m), after which turbulence statistics were reset. Afterwards the model was run for two times that time, collecting statistics for turbulent quantities until reaching equilibrium.

3 MODEL RESULTS AND VALIDATION

A test model without air bubbles was set up and compared with laboratory flume experiments by Decrop *et al.* (2012). The model proved to perform well in reproducing plume trajectories, plume width and turbulent fluctuations of the velocity components and sediment concentration. A sound $-5/3$ power law turbulence cascade for mixture velocity and sediment concentration fluctuations was found after Fourier analysis of the instantaneous flow results (Decrop *et al.*, 2014). Furthermore, it was demonstrated that the resolved turbulent motions account for at least 95% of the total turbulent kinetic energy (resolved + sub-grid scale), a criterion advocated by Pope (2004).

After resizing the laboratory scale model to prototype dimensions, while keeping identical geometry and number of grid points, the performance was evaluated. Obviously, no experimental data is available of the resized flow. When applying the appropriate similarity laws for buoyant plumes, the trajectories of plumes of different dimensions should collapse, given the fact that they own dynamically equivalent properties, namely the densimetric Froude number F_{Δ} and the velocity ratio λ .

$$F_{\Delta}^2 = \frac{W_0^2}{g'D} \quad ; \quad \lambda = \frac{U_0}{W_0} \quad ; \quad g' = g \frac{\rho_m - \rho_w}{\rho_w} \quad (11)$$

with D the overflow shaft diameter, W_0 the shaft exit velocity, U_0 the background flow velocity (sum of sea current and vessel sailing speed) and g' the reduced gravity of the mixture.

After simulation of such plumes of prototype dimensions, but with dynamically equivalent F_{Δ} and λ , the scaled trajectories showed very similar paths. Due to the increase in grid cells size and the higher Reynolds number, the percentage of resolved turbulent kinetic energy dropped. However, it was shown that the resolved turbulent motions still accounted for about 80% of the total TKE, which is considered sufficient.

The LES model presented in this paper was built using identical formulation and numerics as the validated laboratory scale/resized model, with the addition of a realistic TSHD vessel geometry, actuator disks for the propellers and air bubble transport.

In situ measurement data of plume properties have been obtained during two monitoring campaigns in the direct vicinity of TSHD's at work. Results of the campaigns will be compared with model results in this paper, first of a 'shallow' case, secondly for a 'deep water' case. In both campaigns, a hopper dredger at work was followed with a survey boat. A high-speed downcasting SiltProfiler (e.g. Zimmermann *et al.*, 2010) was deployed to take vertical profiles of the sediment concentration at short distance behind the dredging vessel. The advantage over acoustic instruments is that it can be used at this short distance behind the dredger without being affected by air bubbles. These bubbles rendered the acoustic backscatter data collected with an ADCP useless for interpretation to sediment concentration. A series of Optical Backscatter turbidity Sensors was trailed behind the survey boat to monitor sediment concentration closer to the surface. On board the TSDH, mixture samples for suspended solids analysis were taken inside the overflow shaft. Combined with TSHD log sheets (overflow volume discharge) and ambient conditions measurements of U_0 and C , all information for the model boundary conditions was gathered.

For the first (shallow) case, overflow sediment concentration, volume discharge and background sea current velocity were averaged over a 20 minute period and applied as steady boundary condition for LES simulations. The resulting computed plume dilution C/C_0 at the symmetry plane along the vessel's axis is shown in Figure 3. Both in the time-averaged (top) and in the instantaneous (bottom) model result, clearly a bimodal plume can be observed with a dense benthic plume and a more diluted surface plume, separated by a zone with lower turbidity. Near the sea bed, the dense layer has concentrations an order of magnitude higher compared to the surface plume. The surface plume separates from the main plume directly after the exit, where at the outer fringes local eddies detach. These swirls no longer travel downward with the momentum of the main plume, but are under influence of the -at that location- still high air bubble concentration and experience therefore a positive buoyancy, causing the lifting towards the vessel hull.

The initial volume concentration of air bubbles is a parameter which cannot be measured directly in the field. An empirical equation for the air bubble entrainment of surface impinging jets by Ervine (1998) was applied to find a typical value for the considered overflow shaft of $c_a = 7\%$. The influence of the presence of air bubbles on the surface plume was investigated. It is shown that for this specific case, the surface plume sediment concentration increased by a factor four due to the presence of a 7% air bubble concentration (Figure 4a). The presence of air bubbles increases the surface concentration considerably, but the surface plume is not entirely absent without air bubbles in the overflow mixture (as for example during the ideal application of a green valve).

The initial bubble diameter has quite an influence on the resulting surface plume concentrations and is still a parameter with uncertainty. In order to determine a good initial bubble diameter, the vertical profiles of sediment concentration in the plume were compared with in situ measurements by the SiltProfiler. In situ measurements are always a snapshot in a spatially heterogeneous plume, and so is an instantaneous model result. Both snapshots are difficult to compare, therefore the time-averaged model result is compared with a number of measured profiles. With an initial air bubble concentration of 7% it was found that the simulations with an initial air bubble diameter of 2 mm lead to the best match with measured concentration profiles. Figure 4b shows measured and modelled profiles at 240 m behind the dredger. Apart from the surface plume concentration, also the benthic plume with higher concentration is modelled in a satisfactory way. The correct concentration near the bed is found as well as the correct concentration gradient in the first meters above the sea bed. At a distance of 120 pipe diameters (here, 240 m) the initial sediment concentration is diluted by a factor 50 near the bed and a factor 2000 near the surface. The lower turbidity zone in this specific measured profile is a temporary feature, not always found at this distance from the TSHD.

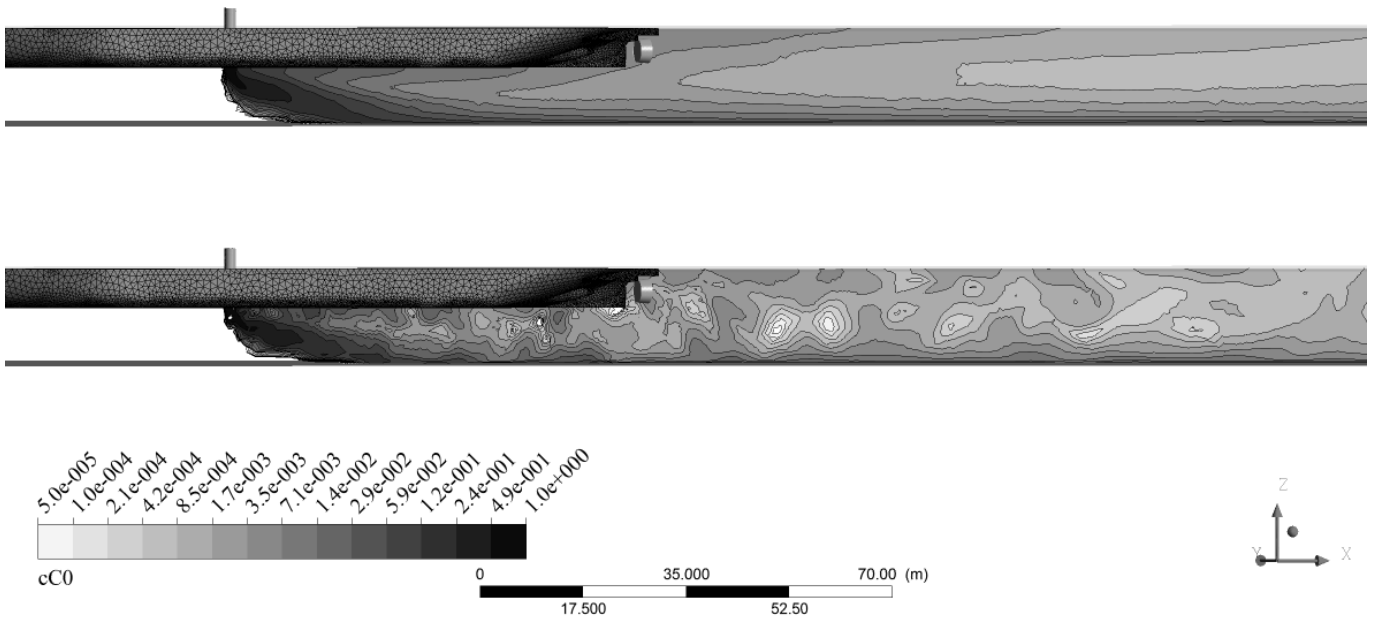


Figure 3. Plume dilution C/C_0 , at the symmetry plane along the axis of the vessel. Time-averaged (top) and instantaneous (below) LES solution.

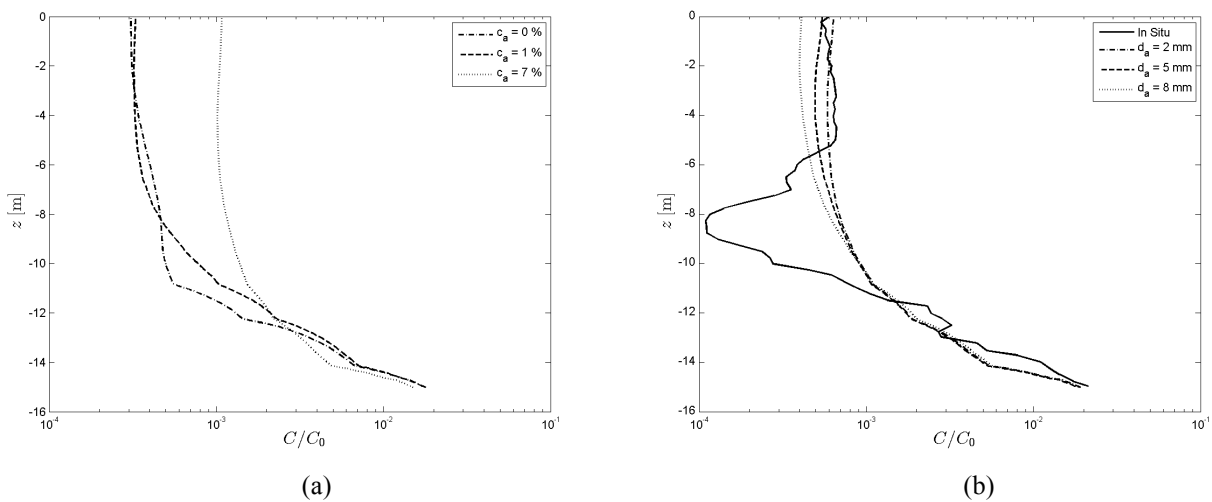


Figure 4. (a) Vertical sediment profiles of simulations with different volume concentration of 2 mm air bubbles (b) Field measurement of a vertical sediment concentration profile (in situ, full line), compared with model results of simulations with different initial air bubble diameter. Profiles at 240 m behind the dredger.

In the current case, the lower turbidity zone between both plumes is also found in the model results (Figure 3), but fades with increasing distance from the overflow pipe exit. Up to a distance of 50 pipe diameters, a clear separation between benthic highly concentrated layer and surface plume is observed in the time-averaged results. At greater distance, the benthic layer still exists, with a more uniform sediment concentration above it, reaching up to the surface. At 400 m behind the overflow, the surface plume was about 60 m wide, while the benthic layer further widened to a width of 180 m, due to the lateral density current developing at the high concentration gradient.

Compared to the first case, the case of the second measurement campaign had much greater water depth (40 m), a narrower overflow pipe which was located closer to the stern. In simulations of this deep water case, the complete plume was located in the top 25 % of the water depth in both model and measurements (not shown). The simulated surface plume concentrations were compared with measured surface plume values for both cases (Figure 5). It can be seen that there exists a large spreading in the measurements, due to local variations and a position of the survey boat relative to the plume centreline changing with time. However, the simulated sediment concentrations seem to be in the good range, compared to the measured concentrations.

When examining the structure of the sediment plume at the surface, indeed a relatively narrow plume is found which reaches a width of roughly twice the vessel width at a distance behind the stern of two times the length of the vessel (Figure 6). In the instantaneous surface plume, internal concentration variations over the width of the plume are caused by the turbulent motions in the LES model. Turbulent variations in the surface plume have a root-mean-squared value of about 60 % of the time-averaged concentrations.

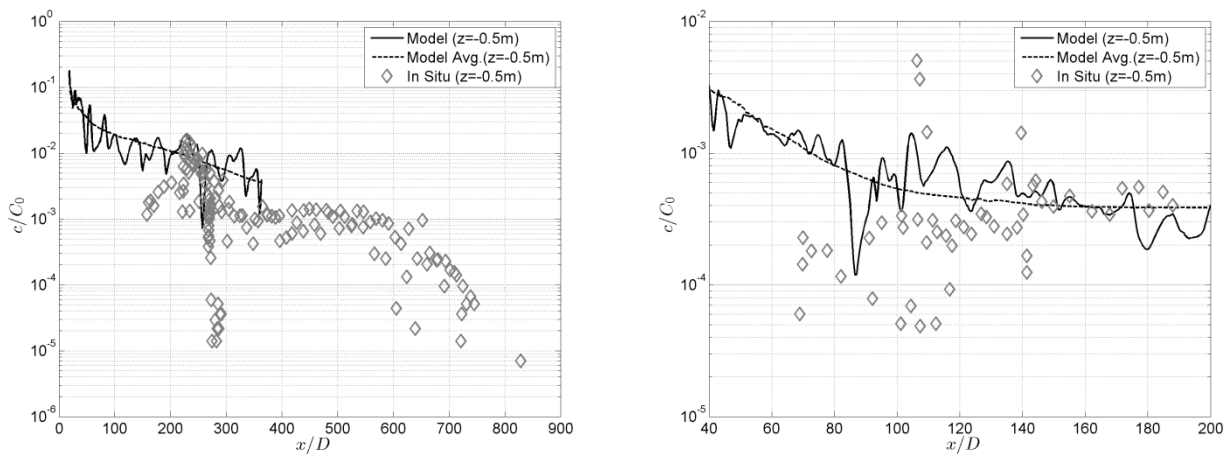


Figure 5. Simulated sediment concentration at the symmetry plane and near the surface (instantaneous in full line, time-averaged in dashed line), versus measured surface values at various locations in the plume (a) for the first case, (b) for the second case.

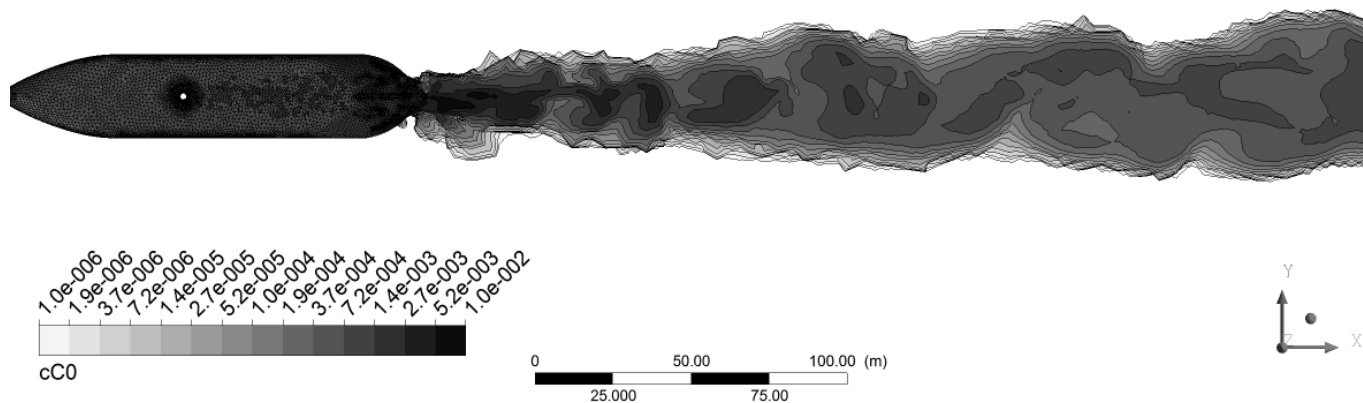


Figure 6. Plume dilution c/C_0 values at the water surface, bird perspective view of the instantaneous LES solution.

4 CONCLUSIONS

A three-dimensional, multi-phase Large-Eddy Simulation model was developed for the simulation of Trailer Suction Hopper Dredgers’ overflow plumes. The model uses a mixture model approach for the sediment-water mixture and a Lagrangian approach for air bubble transport. A realistic geometry of a Trailing Suction Hopper Dredger was incorporated in the model domain as well as the overflow shaft itself. Propeller action is included as a momentum source using the actuator disk method.

Two simulation cases were set up according to measurements of sediment flux in the overflow shaft of a TSHD at work as well as of the conditions of the surrounding sea: one case with deep water (40 m) and one case with more shallow water. In the relatively limited water depth of the shallow case (16 m) and keel clearance (9.5 m), the main plume reaches the sea bed rapidly and forms a benthic density current. A secondary plume is formed due to eddies detaching from the main plume, an effect amplified by the presence of air bubbles. Measured vertical profiles of sediment concentration from sea bed to water surface were compared with simulation results, showing good agreement in both the benthic density current and the surface plumes. Sensitivity tests showed that the presence of air bubbles in the overflow mixture increases the sediment concentration in the surface plume by a factor four in this case. In the deeper water case, the plume was fully located in the top 25 % of the water column in both model and measurements.

The presented near-field model is a suitable tool to determine the fraction of the released sediments becoming part of a diluted far-field plume. These plumes no longer have the initial negative buoyancy of the near-field plume and can travel over great distance with the sea currents, potentially bringing them to ecologically sensitive areas. The near-field sediment distributions calculated by the presented model can as such be used as input for large-scale sediment dispersion models, which can subsequently determine the fate of the far-field plumes.

REFERENCES

- Decrop, B., De Mulder, T., Troch, P., Toorman, E. and Sas, M. (2012) Experimental investigation of negatively buoyant sediment plumes resulting from dredging operations. In: *Coastlab 2012 Proceedings*, 573-582.
- Decrop, B., De Mulder, T. and Toorman, E.A. (2014) Large-Eddy simulations of turbidity plumes in crossflow. Submitted to: *European Journal of Mechanics, B-Fluids*.
- Ervine, D.A. (1998) Air entrainment in hydraulic structures, a review. *Proc. Instn Civ. Engrs Wat., Marit. & Energy*, 1998, 130, Sept, 142-153.
- Fric, T., Roshko, A. (1994). Vortical structure in the wake of a transverse jet. *Journal of Fluid Mechanics* 279, 1-47.
- Germano, M., Piomelli, U., Moin, P., Cabot, W.H. (1991). A dynamic subgrid-scale eddy viscosity model. *Physics of Fluids A: Fluid Dynamics* 3, 1760.
- Hough, G. R. and Ordway, D. E. (1964) The generalized actuator disk, Technical Report TAR-TR 6401, Therm Advanced Research, Inc.
- Kelso, R.M., Lim, T., Perry, A.E. (1996). An experimental study of round jets in cross-flow. *Journal of Fluid Mechanics* 306, 111-144.
- Lilly, D. (1992). A proposed modification of the Germano subgrid-scale closure method. *Physics of Fluids A: Fluid Dynamics* 4, 633.
- Pope, S.B. (2004) Ten questions concerning the large-eddy simulation of turbulent flows. *New Journal of Physics* 6.
- Zimmermann, N., Melotte, J., Breugem, W.A., Sas, M and Leahy, D. (2010) Monitoring the behaviour of sediments disposed by a TSHD In the external estuary of the Loire. In: *Proceedings of the WODCON XIX conference*.